Advances in Concrete Construction, *Vol. 7, No. 1 (2019) 11-22*
DOI: https://doi.org/10.12989/acc.2019.7.1.011

Numerical simulation approach for structural capacity of corroded reinforced concrete bridge

Xuhong Zhou[1], Xi Tu[*1], Airong Chen[2] and Yuqian Wang[3]

[1]*Key Laboratory of New Technology for Construction of Cities in Mountain Area, Chongqing University, Ministry of Education, Chongqing, China*
[2]*Department of Bridge Engineering, Tongji University, Shanghai, China*
[3]*China-Road Transportation Verification & Inspection Hi-Tech Co. Ltd., Beijing, China*

(Received August 21, 2018, Revised December 12, 2018, Accepted December 15, 2018)

Abstract. A comprehensive assessing approach for durability of reinforced concrete structures dealing with the corrosion process of rebar subjected to the attack of aggressive agent from environment was proposed in this paper. Corrosion of rebar was suggested in the form of combination of global corrosion and pitting. Firstly, for the purposed of considering the influence of rebar's radius, a type of Plane Corrosion Model (PCM) based on uniform corrosion of rebar was introduced. By means of FE simulation approach, global corrosion process of rebar regarding PCM and LCM (Linear Corrosion Model) was regressed and compared according to the data from Laboratoire Matériaux et Durabilité des Constructions (LMDC). Secondly, pitting factor model of rebar in general descend law with corrosion degree was introduced in terms of existing experimental data. Finally, with the comprehensive numerical simulation, the durability of an existing arch bridge was studied in depth in deterministic way, including diffusion process and sectional strength of typical cross section of arch, crossbeam and deck slab. Evolution of structural capacity considering life-cycle rehabilitation strategy indicated the degradation law of durability of reinforced arch bridges.

Keywords: reinforced concrete structures; diffusion; corrosion; durability; service life

1. Introduction

Durability is an important issue for long-term operation of reinforced concrete bridge structures, which are usually costly to repair and in light of environmental damage and human safety. The design of bridge structures is achieving the functional purpose of structures within their target service life. In most cases, the degradation of structural capacity of concrete structures relies on the corrosion degree of rebar and related damages within concrete induced by aggressive agent from environment. Decisions regarding the future integrity of a structure or its components, relating to the type, cost, and possible rehabilitation strategy, depend upon an accurate assessment of the process of corrosion and the conditions affecting rate of deterioration (Roberge 2008).

In coastal and marine region steel bar embedded in concrete is considered being in risk of corrosion when alkaline protecting film is depassivated by chloride penetration due to decrease of pH value of pore water or threshold chloride content attained (Papadakis 2013). A complex procedure of electrochemical reaction furthermore induces decrease in effective cross section and ductility of steel bar, cracking of cover concrete by rust expansion, even spalling or delamination. Corrosion process of rebar directly depends on cover depth (boundary condition), the penetration rate of the aggressive agents and its concentration distribution. Though clear model for rebar corrosion and environmental attack has not been created, several important laboratorial experiments have been accomplished. Rodriguez studied the relationship between rebar corrosion and structural performance based on a group of accelerated corrosion experiments (Rodriguez *et al*. 1997). Obtained experimental result indicated that corrosion enhanced structural deflection and cracking of concrete, changed failure type of corroded RC structure and clarified the relationship between deterioration of concrete cover and corrosion. Coronelli (2004), Sanchez (2010) studied Rodriguez's result in-depth, recreated the experimental process by numerical simulation. Gonzalez studied the corrosion patterns of natural corrosion experiments and accelerated corrosion experiments and summarized the range of pitting factor of corroded rebar and discussed the factors affecting the result of accelerated corrosion experiments (González *et al*. 1995). A group of important long-term natural corrosion experiments were finished in LMDC (Laboratoire Matériaux et Durabilité des Constructions de Toulouse) (Castel *et al*. 2000, Vidal *et al*. 2004, Vidal *et al*. 2007, Yu *et al*. 2015, Zhang *et al*. 2009, Zhang *et al*. 2009, Zhu and Francois 2013, Zhu and François 2015, Zhu *et al*. 2016). The results covered the corrosion process up to 27 years and provided the characteristics and time evolution of degradation of reinforced concrete beams, including distribution of pitting corrosion, crack pattern, chloride concentration and structural performance.

*Corresponding author, Ph.D.
E-mail: tuxi@cqu.edu.cn

 ISSN: 2287-5301 (Print), 2287-531X (Online)

Clearly corrosion model for steel bar in concrete is still controversial. Generally, an applicable approach is regression of relationship between chloride content and corrosion rate by means of a group of accelerated and natural corrosion experiment tests (Liu and Weyers 1998, Vidal *et al*. 2007). But these deterministic models based on given condition were not applicable for various cases in engineering application, though it revealed the typical degradation process of reinforced concrete structures.

In light of numerical simulation, Biondini accomplished a series of fundamental research achievement on time-variant durability analysis approach, simulates the diffusion process by the approach of cellular automata providing the easily grid-meshing of domain and reliable efficiency. However, the choice of solving parameters is critical for further unexpected calculating error while the indispensable requirement of regular meshing cause the lower adaption of domain boundary and furthermore lower accuracy. Besides, Biondini (2006) presented a general approach to evaluate the performance of concrete bridges under corrosion based on three-dimensional beam finite element accounting for mechanical and geometrical nonlinearity, considering reduction of cross-sectional area and ductility of rebar, deterioration of concrete strength and spalling of concrete cover. Since pitting corrosion may involve a significant reduction of steel ductility, Biondini summarized the ductility reduction model of reinforcing steel based on previous experimental data describing the relationship between steel ultimate strain and damage index of rebar (Biondini and Vergani 2012).

At present it is reasonable to model a deterministic analysis approach for the entire process of corroded reinforced concrete structures based on available experimental data and summarized physical laws. This paper presented an optimized damage models for concrete and rebar combined with FE simulation approach and summarized an adaptable corrosion model for steel bar based on introduced assessing approach and available experimental data. Accordingly, the degradation process of an aged concrete arch bridge and its major structural members was discussed.

2. Diffusion model of numerical simulation

The penetration of chloride ion has been considered as the major reasons for corrosion of rebar in concrete. It was recognized as the diffusion of ion in in porous material as form of differential equation, which is always described by Fick's law (Yuan *et al*. 2009)

$$\partial\phi/\partial t = \nabla^2\phi \tag{1}$$

Where, ϕ denotes chloride content in concrete.

Besides, binding effect decrease effective chloride content on surface of rebar and thus chloride diffusivity (Thoft-Christensen 2002). In cases of the presence of chloride binding, the bound chloride ion will be from the diffusion flux and can be subtracted from the conservation of mass equation

$$\omega_e\left(\partial c_f/\partial t\right) = \nabla\left(D_e\omega_e\nabla c_f\right) - \partial c_b/\partial t \tag{2}$$

$$c_t = c_b + c_f\cdot\omega_e \tag{3}$$

Where c_f is free chloride concentration (kg/m^3 solution), c_b is bound chloride concentration (kg/m^3 concrete), c_t is total chloride concentration (kg/m^3 concrete), and D_e is effective diffusion coefficient (m^3/s). ω_e is evaporable water content (m^3 solution/m^3 concrete). Generally, binding effect of chloride in concrete is described as the function of free chloride content, which was calculated by binding isotherm, such as Freundlich isotherm (Martín-Pérez *et al*. 2000)

$$c_b = \alpha c_f^{\ \beta},\ \frac{\partial c_b}{\partial c_f} = \alpha\beta c_f^{\ \beta-1},\ \frac{D_a}{D_e} = \frac{\omega_e}{\omega_e + \alpha\beta c_f^{\ \beta-1}} \tag{4}$$

For general environmental condition. α=1.03. β=0.36. According to (4), apparent chloride diffusivity regarding bonding effect relates to free chloride content and thus nonlinear process of chloride diffusion can be observed.

The effects of temperature can be estimated by correcting a reference diffusion coefficient (Bastidas-Arteaga *et al*. 2011)

$$D(T) = D_{ref}\cdot\exp\left[\frac{U}{R}\cdot\left(\frac{1}{T_{ref}} - \frac{1}{T}\right)\right] \tag{5}$$

Where, D_{ref} is chloride diffusivity at reference temperature T_{ref}, U is activation energy of the chloride diffusion process (U=35000 J/mol), R is gas constant (R=8.3145 J/(mol·K)).

In terms of solving Fick's law, Cellular Automata is not suitable for irregular shape, size and boundary of analyze region due to its uniform background meshing grid. Considering the thickness of concrete cover compared with overall dimension of concrete member, significant error on chloride content cannot be ignored. Therefore, FEA approach based on free meshing and isoparametric formulation is considered as an appropriate approach. Numerical implementation of chloride diffusion based FEA was discussed as followed. Assuming constant chloride diffusivity D_a during duration time, t. If considering constraint condition $\phi = \bar{\phi}$ on boundary Γ, equivalent integral form of differential equation for transient chloride diffusion content ϕ is

$$\int_\Omega\left[\delta\phi\left(\partial\phi/\partial t\right) - D_a\nabla^2\phi\right]d\Omega = 0 \tag{6}$$

Within the n nodes element in discrete region Ω, chloride content ϕ can be interpolated by nodal value ϕ_i and is expressed as the function of time t

$$\phi = \sum_{i=1}^{n} N_i(x)\phi_i(t) \tag{7}$$

Where, N_i is shape function for each element.

Defining **K** as chloride diffusion matrix and **C** as chloride capacity matrix, elements of which are expressed as followed

$$K_{ij}^e = \int_{\Omega^e}\left(D_a\frac{\partial N_i}{\partial x}\frac{\partial N_j}{\partial x} + D_a\frac{\partial N_i}{\partial y}\frac{\partial N_j}{\partial y}\right)d\Omega \tag{8}$$

$$C_{ij}^{e}=\int_{\Omega^{e}} N_i N_j d\Omega \tag{9}$$

Assuming constant **K** and **C** during each time step Δt, a general form of (6) is expressed

$$\left(\mathbf{C}/\Delta t+\mathbf{K}\theta\right)\mathbf{\Phi}_{n+1}+\left[-\mathbf{C}/\Delta t+\mathbf{K}\left(1-\theta\right)\right]\mathbf{\Phi}_{n}=0 \tag{10}$$

Where, $\mathbf{\Phi}_n$ and $\mathbf{\Phi}_{n+1}$ are the nodal chloride content at time t_n and t_{n+1} respectively. Here, θ=1/2 is adopted for central-difference formulas. A more familiar form of (10) is

$$\bar{\mathbf{K}}\mathbf{\Phi}_{n+1}=\bar{\mathbf{Q}}_{n+1} \tag{11}$$

Where, $\bar{\mathbf{K}}=\mathbf{C}/\Delta t+\mathbf{K}\theta$ and $\bar{\mathbf{Q}}_{n+1}=\left[\mathbf{C}/\Delta t-\mathbf{K}\left(1-\theta\right)\right]\mathbf{\Phi}_{n}$. Based on (11), $\mathbf{\Phi}_{n+1}$ can be solved by available $\mathbf{\Phi}_n$ and material properties of concrete.

For nonlinear diffusion regarding binding of concrete, for each time-step of transient solving process, chloride content within the entire domain is solved and apparent chloride diffusivity of each element, D_a, is updated according to (4)

3. Corrosion model of reinforcement

Corrosion by the presence of chloride on surface of rebar induced is a complex electrochemical reaction between anode and cathode. Localized depassivation of rebar firstly occurs due to concentration of chloride ion and then galvanic corrosion between anode (exposed rebar) and cathode (passive film). Furthermore, electric potential drives the movement of chloride ion, enhances corrosion process and pitting of rebar appears. Corrosion process and pattern are rather complex referring to the porosity and binder type of concrete, surrounding boundary condition and external loading. Experimental research indicated that corrosion degree was highly indeterminate longitudinally along steel bar and difficult to be accurate predicted considering loading and chloride penetration (Yu *et al*. 2015). By far a simple and implicit model describing the corrosion process of rebar with distribution of chloride in concrete can hardly be provided by means of experiment and case study of structures in long-term service.

A commonly acceptable assumption was introduced that the corrosion form of rebar is composed of two parts. Global Corrosion (uniform corrosion index, δ_A) describes the overall corrosion index of a certain length of rebar. Uniform corrosion index δ_A was expressed as below

$$\delta_A=\Delta m_s/m_{s,0}=\Delta A_s/A_{s,0}=\left(A_{s,0}-A_s\right)/A_{s,0} \tag{12}$$

Where, $m_{s,0}$ and $A_{s,0}$ denote initial total weight and initial area of cross section of the segment of rebar respectively. Δm_s and $A_{s,0}$ denote mass loss and area loss of cross section of corroded rebar. For the consideration of localized corrosion, pitting factor R is defined as the ratio between maximum cross-sectional loss and average cross-sectional loss. Thus, pitting Corrosion (pitting corrosion index $\delta_{A,pit}$) was expressed as below

$$\delta_{A,pit}=\delta_A\cdot R \tag{13}$$

Corrosion model and pitting corrosion model for steel bar were discussed in follow content of this paper based on (12) and (13).

3.1 Global corrosion model

In macroscale, rebar was simplified as a dimensionless point in concrete. Corresponding chloride content surrounding rebar was extracted at the centroid of rebar from result of FE numerical simulation. Biondini (Biondini *et al*. 2006) introduced an approximate Linear Corrosion Model (LCM) for corrosion of rebar under aggressive agent evaluating corrosion speed by current chloride concentration at rebar and related coefficients

$$\partial\delta_A\left(\mathbf{x},t\right)/\partial t=\phi\left(\mathbf{x},t\right)/\phi_s\Delta t_s=k_L\phi\left(\mathbf{x},t\right) \tag{14}$$

Where, $\delta_A(\mathbf{x},t)$ denotes dimensionless sectional corrosion index, $\delta_A=(A_{s,0}-A_s)/A_{s,0}$. C_s represents the values of constant concentration $C(\mathbf{x},t)$ leading to a complete corrosion of the materials after the time periods Δt_s and $k_L=1/C_s\Delta t_s$. The above linear corrosion model does not consider rebar's diameter and thus without available data by experiments the linear damage factor k_L is not applicable for any type of rebar.

In this paper, a type of Plane Corrosion Model (PCM) based on assumption of uniform corrosion on surface of rebar was introduced (Fig. 1). Corrosion process of rebar was simplified and defined as uniform plane between steel and aggressive environment. It is acceptable to assume the uniform corrosion process with the equally distribution of aggressive agent on the surface, which defines as Plane Corrosion.

Thus, the induced thickness of corrosion layer ΔR after a given time Δt corresponding to the concentration of aggressive agent C is determined by a linear model of plane corrosion suggested as follow

$$\Delta R=f\left(C\left(\mathbf{x},t\right),\Delta t\right)=k_P\cdot C\left(\mathbf{x},t\right)\Delta t \tag{15}$$

Where, k_P is the plane corrosion factor. For the rebar with initial radius of R_0, corrosion rate can be expressed by the ratio of area lost to initial area.

$$\Delta\delta_A=\frac{\Delta A_s}{A_{s,0}}=\frac{2\pi R\cdot k_P C\left(\mathbf{x},t\right)\Delta t}{\pi R_0^{\,2}}=\frac{2Rk_P}{R_0^{\,2}}C\left(\mathbf{x},t\right)\Delta t \tag{16}$$

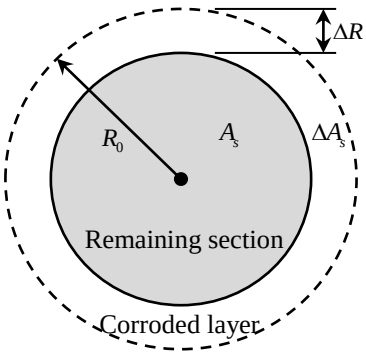

Fig. 1 Uniform corrosion of steel rebar

Table 1 Analysis of experimental data from LMDC

Time (year)	$\Delta R/\Delta t$ (mm^2/year)	$\Delta\delta_A/\Delta t$ (1/year)	$\bar{\phi}_t$ (%w)
0~5	0.000	0.0000	0.000
5~14	0.288	0.0025	0.178
14~23	0.604	0.0053	0.305
23~26	0.842	0.0074	0.315
26~28	2.935	0.0259	0.319

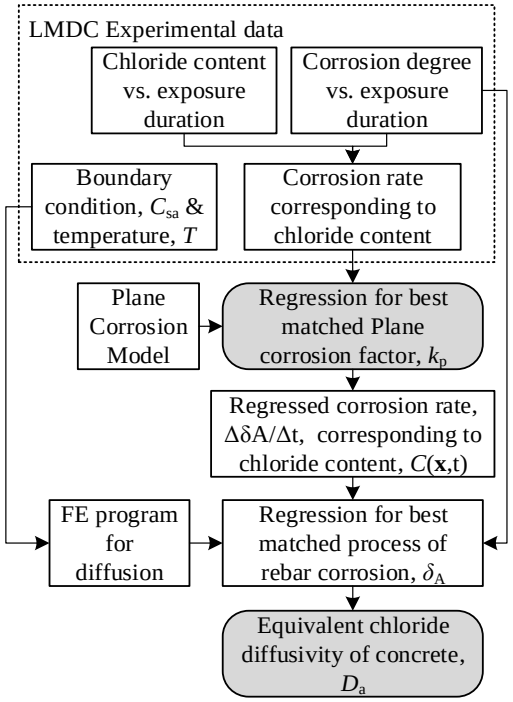

Fig. 2 Regression for plane corrosion factor and equivalent chloride diffusivity

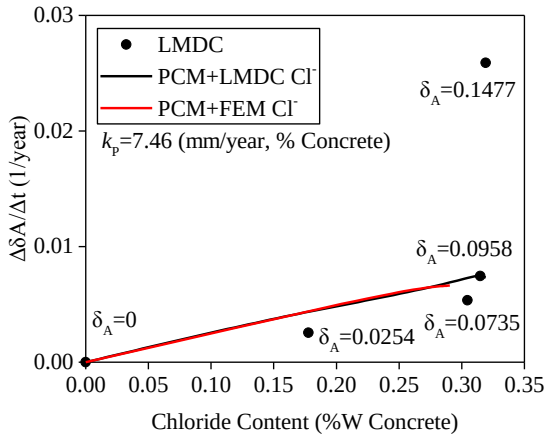

Fig. 3 Corrosion rate vs. chloride content of fitting model based on LMDC experimental data

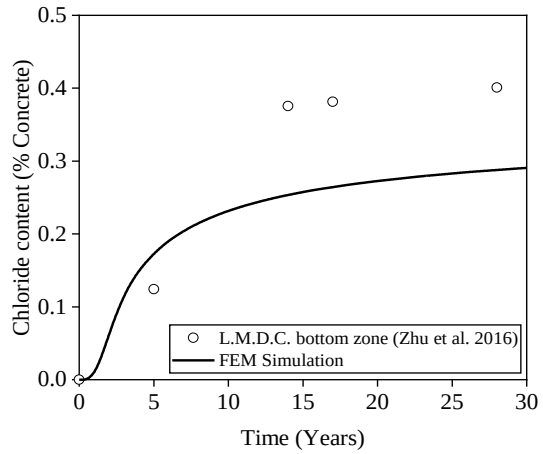

Fig. 4 Chloride content evolution of LMDC experimental data and numerical simulation

$$\frac{\Delta\delta_A}{\Delta t}=\frac{2Rk_P}{R_0^{\,2}}C(\mathbf{x},t) \tag{17}$$

Where, R is the radius of corroded rebar and $R/R_0=\sqrt{1-\delta_s}$. Therefore, corrosion rate was expressed as below

$$\frac{\Delta\delta_A}{\Delta t}=\frac{2k_P}{R_0}C(\mathbf{x},t)\sqrt{1-\delta_A} \tag{18}$$

As the major factor of corrosion process of rebar, corrosion factor k_P was always obtained by means of analytical assessment and experimental test. Firstly, for analytical assessment, physiochemical reaction and time evolution of rebar corrosion was assessed regarding material properties of steel and concrete, environmental parameters and loading factor in accurate and quantitative approach (Liu and Weyers 1998). Secondly, for the approach of experimental test, equivalent corrosion process of rebar was regressed by available experimental data and therefore complex analytical assessment avoided, which was applicable for general engineering design.

In order to evaluate lifetime structural capacity of concrete structures, optimized model describing remaining effectiveness of rebar was discussed in this paper. Based on experimental data from LMDC (Zhu and François 2015, Zhu *et al*. 2016), corrosion factor of plane corrosion model k_P was regressed by means of comprehensive FE simulation. Reorganized corrosion rate and chloride content of LMDC experiment was list in Table 1.

Fitting process for corrosion model based on LMDC experimental result was shown in Fig. 2. According to Fick's law, a two-variable regression analysis was studied. By means of modifying plane corrosion factor k_P and apparent diffusivity of concrete D_a, a corrosion process of rebar by numerical simulation which fit the data from LMDC experiment was obtained.

For the study of regression, firstly, time evolution of chloride content at the depth of 16mm from surface of concrete was calculated by numerical simulation approach introduced in this paper. Concrete composition was referred from LMDC (Zhu and François 2015). Chloride content at bottom of beam where being tensioned was calculated in terms of stress distribution of general reinforced concrete bridges. Boundary condition of numerical simulation was defined based on actual configuration of LMDC experiment, including salt-spray laboratory environment (0~6 years), wetting-drying cycles (6~9 years), outdoor

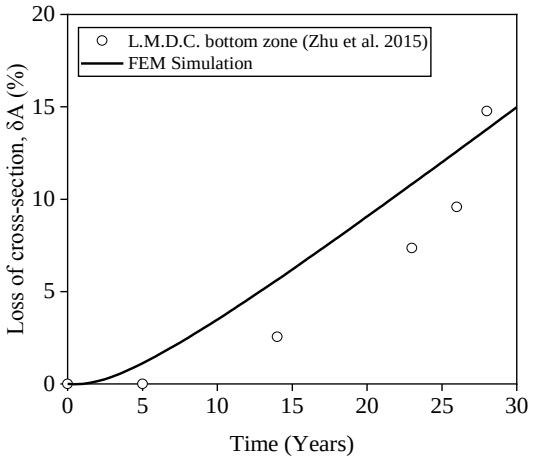

Fig. 5 Rebar corrosion evolution of LMDC experimental data and numerical simulation

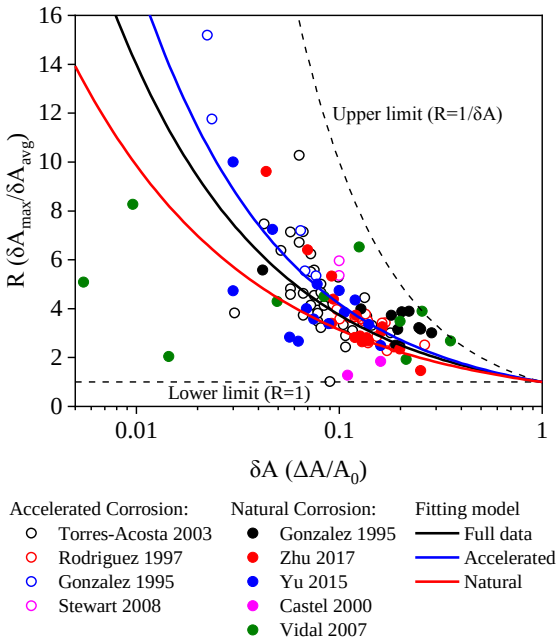

Fig. 6 Pitting corrosion model of steel rebar

wetting-drying cycles (9~19 years), outdoor environment (19~26 years) and outdoor wetting-drying cycles (from 26 years).

Chloride content on surface of concrete is 0.14% (weight ratio in concrete). Temperature of chloride diffusion was considered as the ambient outdoor temperature of southwest France. Linear isotherm for bounding of chloride ion in concrete was adopted. the ratio between bounded and free chloride ion was assumed as 1.5 (Zhu *et al*. 2016).

Regressed relationship between corroding rate of rebar vs. chloride content was shown in Fig. 3. Fitting time evolution of chloride content based on LMDC experiment data was shown in Fig. 4. Corrosion process of rebar was calculated in terms of obtained plane corrosion factor and chloride content, shown in Fig. 5. By means of comprehensive FE simulation, plane corrosion factor was suggested as k_p=7.461 mm/year,%w. Corresponding apparent chloride diffusivity in concrete was D_a=1.62×10^{-12} m^2/s. It was worth noting the significant difference between experimental data and result from numerical simulation, shown in Fig. 4. The major reason is the simplified regression law proposed and only one parameter k_p was involved, which can hardly describe the complex process of corrosion. In this paper, matching the overall regression law of corrosion or loss of cross-section was the main object and thus the deviation in the middle could be ignored.

3.2 Pitting model

Pitting of rebar has been recognized as the non-uniform corrosion, which is highly indeterminate of distribution. According to experimental result, strength and ductility of rebar are significantly weakened by pitting (Cairns *et al*. 2005). For describing pitting degree, pitting factor (R) was expressed as the ratio of maximum corrosion degree corresponding to global corrosion degree of an individual rebar. Thus, the reduced area of corroded rebar was calculated based on the initial diameter of rebar, average corrosion index and pitting factor

$$A_{s,\mathrm{pit}} = (1-\delta_A R) A_s \tag{19}$$

The process of non-uniform corrosion of steel bars is divided into two stages (Zhang *et al*. 2010): 1) for the initial stage, corrosion pit disperse throughout the steel bar longitudinally while the rest surface of steel bar remain being protected by passive film. Thus the average corrosion index remains low and pitting factor increases high. The upper limit of pitting factor is $R_{\uparrow}=1/\delta_A$; 2) After a certain period of service time, with increasing of corrosion depth on the whole surface of steel bar, pitting factor decreases. The lower limit of pitting factor is $R_{\downarrow}=1$. The limit range of pitting factor was drawn as the dashed lines in Fig. 6. According to Yu's experimental results (Yu *et al*. 2015), pitting factor ranged from 2 to 10.

Referring to currently available experimental data listed in Fig. 6 (Castel *et al*. 2000, González *et al*. 1995, Rodriguez *et al*. 1997, Stewart and Al-Harthy 2008, Torres-Acosta Andrés and Martı´nez-Madrid 2003, Vidal *et al*. 2007, Yu *et al*. 2015, Zhu *et al*. 2017), simplified pitting corrosion model based on logarithmical function by mathematical fitting is expressed as below:

For all data (Fig. 6 Black line),

$$R = \delta_A^{-0.573} \quad (0 \le \delta_A \le 1) \tag{20}$$

For accelerated corrosion experiment (Fig. 6 Blue line),

$$R = \delta_{A,Accelerated}^{-0.623} \quad (0 \le \delta_A \le 1) \tag{21}$$

For natural corrosion experiment (Fig. 6 Red line),

$$R = \delta_{A,Natural}^{-0.497} \quad (0 \le \delta_A \le 1) \tag{22}$$

Apparently, as shown in Fig. 6, pitting factor fit from natural corrosion experiment was slightly higher compared with accelerated. Therefore, maximum corrosion index $\delta_{A,\mathrm{pit}}$ can be calculated as below:

For all data (Fig. 7 Black line),

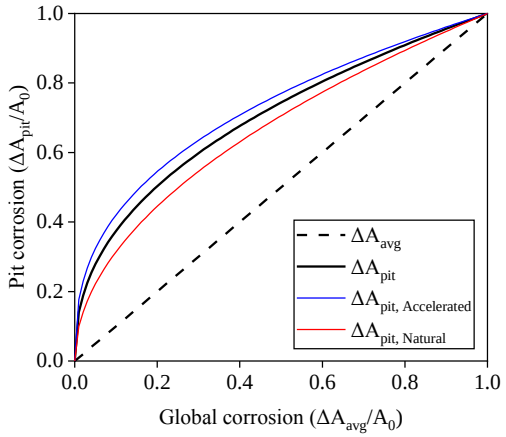

Fig. 7 Relationship between pitting corrosion and uniform corrosion of steel rebar

$$\delta_{A,\text{pit}} = R \cdot \delta_A = \delta_A^{0.427} \tag{23}$$

For accelerated corrosion experiment (Fig. 7 Blue line),

$$\delta_{A,\text{pit}} = R \cdot \delta_A = \delta_A^{0.377} \tag{24}$$

For natural corrosion experiment (Fig. 7 Red line),

$$\delta_{A,\text{pit}} = R \cdot \delta_A = \delta_A^{0.503} \tag{25}$$

4. Implementation of structural assessment of corroded concrete structures

The fiber model was suggested to analyze nonlinear beam element more accurately and integrally, which is suitable for corroded reinforced concrete member (Biondini *et al*. 2004). Stiffness of reduced rebar and cracked concrete were included within element stiffness matrix of degraded beam by means of numerical integration. Implementation of fiber model was discussed as followed.

Stiffness matrix of each beam element $\mathbf{K}_e$ was composed by structural stiffness matrix $\mathbf{K}_M$ and geometric stiffness matrix $\mathbf{K}_G$

$$\mathbf{K}_e = \mathbf{K}_M + \mathbf{K}_G \tag{26}$$

Assuming longitudinal direction of beam as x axis. By integration over the length l of the beam, we obtained

$$\mathbf{K}_M = \int_0^l \mathbf{B}^T \mathbf{H} \mathbf{B} dx \tag{27}$$

$$\mathbf{K}_G = \mathbf{P} \int_0^l \mathbf{G}^T \mathbf{G} dx \tag{28}$$

Where, $\mathbf{P}$ is axial force of beam member. N is shape function. $\mathbf{B}$ and $\mathbf{G}$ are overall strain matrix and bending strain matrix for respectively. The secant stiffness matrix $\mathbf{H}$ was composed by two parts, including concrete part $\mathbf{H_c}$ and steel rebar part $\mathbf{H_s}$, which were calculated by sectional integration of summation.

$$\mathbf{H} = \mathbf{H_c} + \mathbf{H_s} = \int_A \bar{E}_c \mathbf{L}_c{}^T \mathbf{L}_c dA + \sum_{i=1}^{n} \bar{E}_{si} \mathbf{L}_{si}{}^T \mathbf{L}_{si} A_{si} \tag{29}$$

Where, $\bar{E}_c$ and $\bar{E}_{si}$ are secant modulus of the concrete fiber at (x_c,y_c,z_c) and secant modulus of ith rebar placed at (x_s,y_s,z_s) respectively. By means of nonlinear iteration, these secant moduli were calculated by newly obtained nodal displacement, which described the nonlinear change of material under loading. A_{si} is the effective area of cross section of ith rebar. n is the total number of longitudinal rebar within concrete section. $\mathbf{L}$=[1 $-y$ $-z$] is sectional coordinate operator for concrete fiber and rebar.

Considering corrosion degree of rebar $\boldsymbol{\delta}_A$, degradation of material and cross section were expressed as below

$$\mathbf{A}_s = \mathbf{A}_s(\boldsymbol{\delta}_A) \quad \boldsymbol{\varepsilon}_{su} = \boldsymbol{\varepsilon}_{su}(\boldsymbol{\delta}_A) \quad \mathbf{f}_c^* = \mathbf{f}_c(\boldsymbol{\delta}_A) \tag{30}$$

Thus, secant stiffness matrix of corroded reinforced concrete section $\mathbf{H}(\mathbf{x}, \boldsymbol{\delta}_A)$ and degraded concrete section of beam element $\mathbf{K}_e(\boldsymbol{\delta}_A)$ were obtained.

The equilibrium condition of the beam element can be derived

$$\mathbf{K}_s \mathbf{q} = \mathbf{F} \tag{31}$$

Where, $\mathbf{K}_s$=$\mathbf{K}_s(\boldsymbol{\delta}_A)$ is system stiffness matrix of corroded reinforced concrete structure regarding corrosion vector $\boldsymbol{\delta}_A$ of all included steel rebar. $\mathbf{q}$ represents nodal displacement vector. $\mathbf{F}$ is nodal force vector.

5. Discussion of aged concrete arch bridge

A reinforced concrete arch bridge in eastern coastal area of China built in 2000 was studied by means of the approach introduced in this paper (Fig. 8). Recent

Fig. 8 Landscape of reinforced concrete arch bridge

Fig. 9 Visible concrete spalling induced by corroded rebar on lateral surface of deck

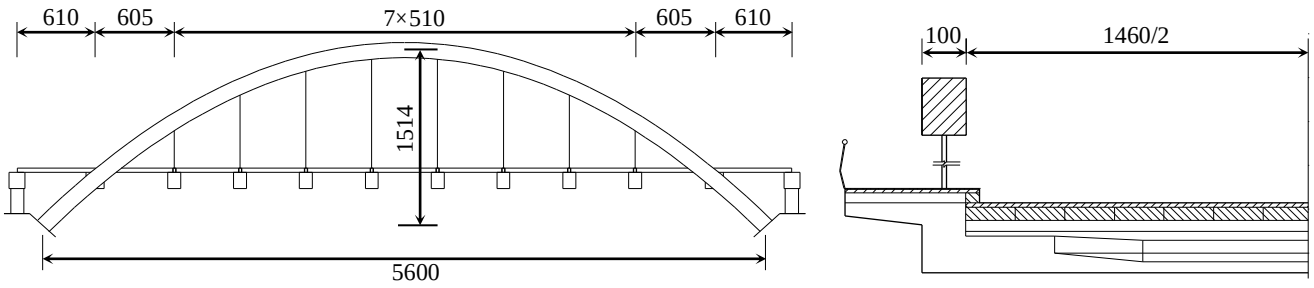

(a) Plan view (b) Cross section of girder

Fig. 10 Dimension and configuration of reinforced concrete arch bridge (Unit: cm)

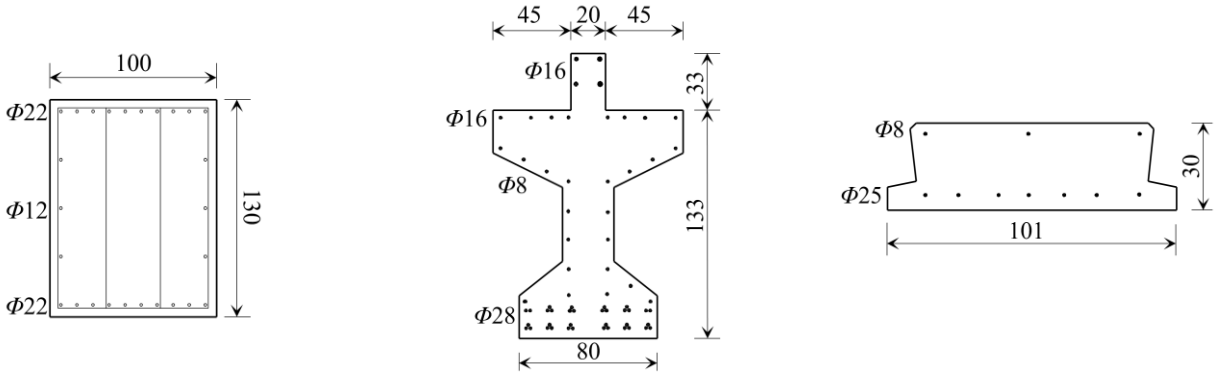

(a) Arch (b) Crossbeam (c) Deck slab

Fig. 11 Section configurations of members (Unit: dimension in cm and rebar diameter in mm)

investigation indicated its weakened structural performance and thus durability evaluation was considered for further assessment (Fig. 9). Suspenders were entirely replaced at 11 years of its service life.

5.1 Model configuration

The total span, height and width of deck are 56m, 15.14m and 14m respectively (Fig. 10). The members of arch bridge were categorized as four major types: arch, suspender, crossbeam and deck slab. The section dimension was shown in Fig. 11. Cross section of each suspender is 0.001649m^2. The FEM model was created as shown in Fig. 18.

For numerical simulation, the stress-strain diagram of the concrete is shown in Fig. 12(a). The branch in compression is described by Saenz (Ascione *et al*. 2005) as followed

$$\sigma_c = -\frac{k\eta - \eta^2}{1+(k-2)\eta} f_c \quad (\varepsilon_{cu} \le \varepsilon_c \le 0) \tag{32}$$

Where, $k=E_{c0}\varepsilon_{c1}/f_c$ and $\eta=-\varepsilon_c/\varepsilon_{c1}$. The branch in tension is defined by an elastic-perfect plastic model. The stress-train diagram of reinforcing steel is assumed elastic perfect-plastic in both tension and in compression (Fig. 12(b)). Detailed parameters for materials of concrete member and suspender were listed in Table 2. Density of concrete and steel were 2500 kg/m^3 and 7850 kg/m^3 respectively.

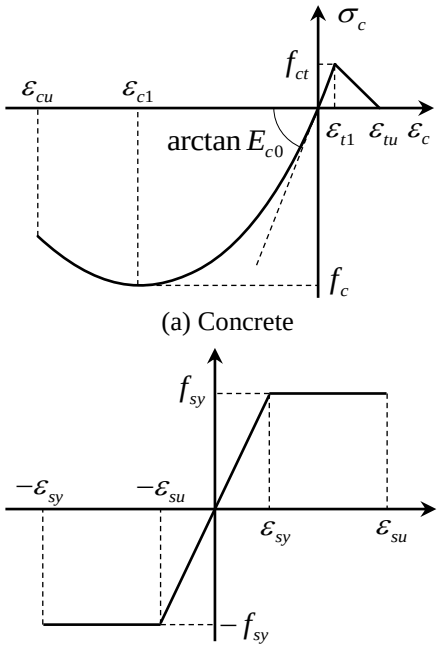

(a) Concrete

(b) Reinforcement

Fig. 12 Diagram of constitutive law for concrete and reinforcement

Chloride diffusion within concrete was assumed as the major factor of determining the long-term structural performance. As deduced in section 0, corrosion factor in light of PCM for rebar was k_P=8.15×10^{-17} m^4/gs. Pitting

Table 2 Mechanical properties of materials for reinforced concrete arch bridge

Member	Detail
Arch	$f_c = 26.8$ MPa, ε_{c1} =0.002, $E_{c0} = 3.25\times10^{10}$ N/m^2, $f_{sy} = 400$ MPa, $E_s = 2\times10^{11}$ N/m^2
Crossbeam, Deck	$f_c = 20.2$ MPa, ε_{c1} =0.002, $E_{c0} = 3.25\times10^{10}$ N/m^2, $f_{sy} = 335$ MPa, $E_s = 2\times10^{11}$ N/m^2
Suspender	$f_u = 1560$ MPa, $E_s = 1.95\times10^{11}$ N/m^2

of rebar was also considered. Ductility of rebar was modified in terms of the model introduced by Biondini (Biondini and Vergani 2012). Material properties of arch bridge were listed in Table 2. Degradation of the compressive strength of concrete was analyzed according to the model introduced by Coronelli (Coronelli and Gambarova 2004). Only ultimate strength of concrete cover confining rebar was considered to be weakened with the development of crack led by expansion of rebar corrosion (Vidal *et al*. 2004). The performance of suspender over service life is unreliable due to fatigue and environmental attack. According to Xu's damage model, due to environmental corrosion, ultimate strength of suspender was in descending linear relationship with time (Xu and Chen 2013). Thus it was simply assumed that suspender completely fails at 40-years' service life and a linear law was adopted to describe the degradation evolution. Failure of anchor was ignored. Since gravity was considered, the density of concrete and steel are assigned as 2500 kg/m^3 and 7850 kg/m^3.

For the numerical simulation, content on surface of concrete member and diffusivity of chloride ion were referred from on-site investigation result on a reinforced concrete pier in eastern coastal region of China (Zhang and Zhang 2017, Zhao *et al*. 2009). Essential parameters were obtained by least square regression method based on analytical solution of Fick's second law. The best matched apparent surface chloride content is 0.708 (% w_c) and apparent chloride diffusivity is 1.837×10^{-12} m^2/s.

Configuration of boundary condition of each types of concrete members were different.

- For arch, due to its completely exposure to atmosphere environment, the entire outline of the cross section of arch was subjected to ingression of chloride ion.
- For crossbeam, both lateral sides and bottom side were exposed. The ingression of chloride ion was ignored at its upper side due to its combination with deck slab and pavement.
- For deck slab, only bottom side was exposed. Its upper side was assumed to be protected by sealing layer from atmosphere.

Environmental temperature was controlled by the model from Bastidas-Arteaga (Bastidas-Arteaga *et al*. 2011). Higher and lower limit of annual temperature were referred to the record of local weather station.

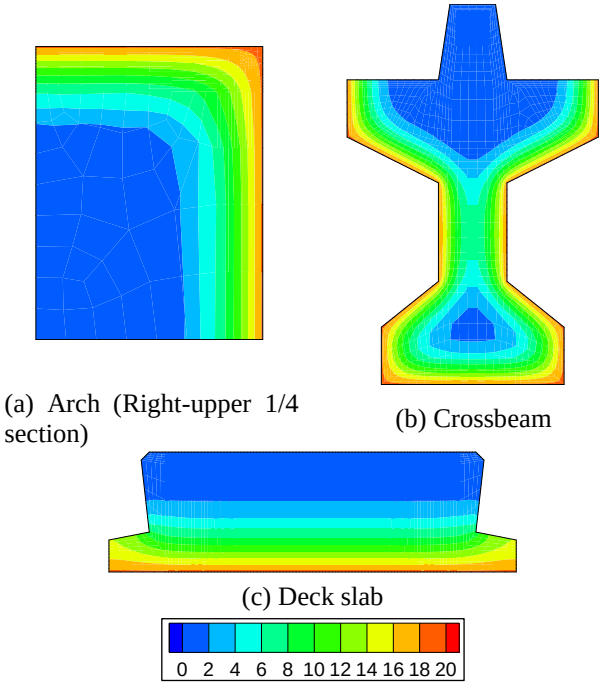

(a) Arch (Right-upper 1/4 section) (b) Crossbeam (c) Deck slab

Fig. 13 Sectional distribution of chloride content of each member, 100 years of exposure (Unit: kg/m^3)

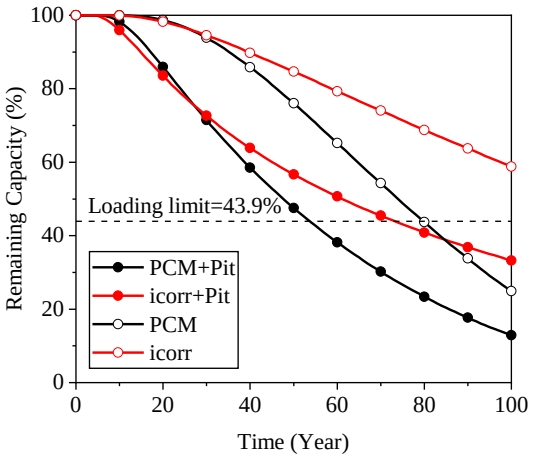

Fig. 14 Remaining capacity of crossbeam over 100 years of exposure

5.2 Structural capacity of members

Chloride content for each type of components at 100 years were obtained by numerical simulation. The contours of sectional chloride distribution were shown in Fig. 13. Corrosion process of each rebar was calculated by corrosion model described by Eqs. (18) and (20) according to PCM approach.

Regarding the structural condition of pure bending, ultimate bending capacity of crossbeam and deck over 100 years' service life were assessed only, shown in Fig. 14 and Fig. 15.

According to the design specification, the loading limit in terms of minimum capacity of each member was controlled by self-weight and traffic loading, shown as the dashed line in the figures.

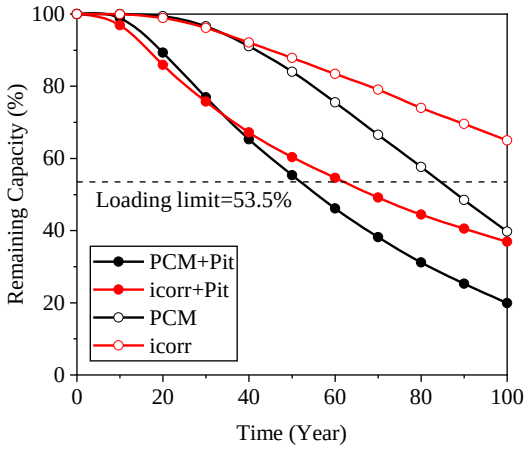

Fig. 15 Remaining capacity of deck slab over 100 years of exposure

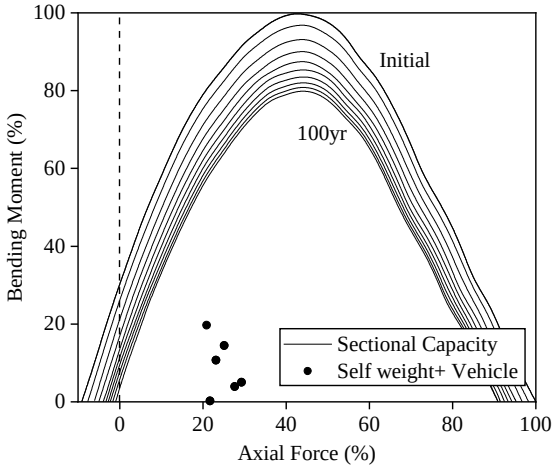

Fig. 16 Remaining capacity of arch over 100 years of exposure (Solid lines) and in-service loading effect (Dots)

Additionally, degradation processes regarding corrosion current induced by given content of chloride ion, based on Liu's model (Liu and Weyers 1998), were also evaluated for comparison (Indicated as icorr in the figures). Result indicated that slight difference of both corrosion models in initial stage was observed. Beyond 30 years of service period, corrosion rate of PCM accelerated and caused deeper corrosion degree and weaker bending capacity. Moreover, pitting caused more corrosion and was proved as the critical factor.

Considering arch behaving as a beam-column due to self-weight and vehicle loading, axial load–bending moment relationship of cross section of arch was calculated combining PCM and pitting model (Solid lines in Fig. 16). Meanwhile, in-service loading effects were calculated and extracted from each combination of nodal internal force on arch (Dots in Fig. 16), which were wholly encased by allowable capacity. Thus, these result verified no failure or major damage would occur in arch due to designed traffic loading throughout the entire service life.

A further question for the systematic capacity is the degradation of suspender. Time-dependent evolution of capacity of suspender, $P(t)$, was simply assumed as a

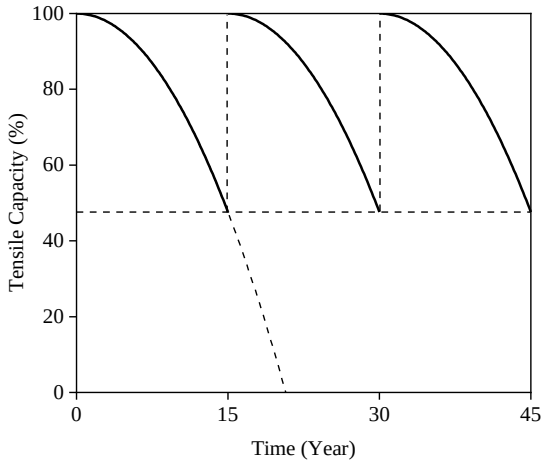

Fig. 17 Remaining relative capacity of suspender

parabola model which was defined by initial ultimate capacity of suspender (P_0), cable force due to designed traffic loading (P_L), average cable replacement interval or design service life of cable (t_1)

$$P(t) = -(P_0 - P_L)t^2 / t_1^2 + P_0 \tag{33}$$

Here, a typical service life of t_1=15*yr* was adopted (Chen *et al*. 2010). Based on the available material parameters, the time-evolution law of degraded suspender was calculated and expressed as a piecewise function, as shown in Fig. 17. Wherein, the solid line denotes the remaining relative capacity of the suspender.

5.3 Failure modes

Maximum structural capacity relates to structural failure mode, which is determined by the weakest member. The failure of any member of the arch bridge would interrupt the load path and hence cause the overall failure of the bridge. Since road bridge mainly subjects to dead load of self-weight and vehicle load, structures were validated by the following general criteria

$$R \geq Q = Q_{DL} + Q_{LL} \tag{34}$$

Where, R denotes structural resistance; Q, Q_{DL} and Q_{LL} represents total load effect, dead load effect and live load effect respectively. Live load effect was calculated in terms of Chinese design specification. In order to simplify the assessment of arch bridge and evaluate the remaining structural capacity, Vehicle Loading Factor, γ, was defined, which was expressed as the ratio of residual resistance structural to live load

$$\gamma = (R - Q_{DL}) / Q_{LL} \tag{35}$$

An accident live load matching the vehicle loading factor over γ would cause the failure of target members or probably the entire failure of the structure. In other words, vehicle loading factor indicates the remaining capacity in service.

The damage of either member would cause the

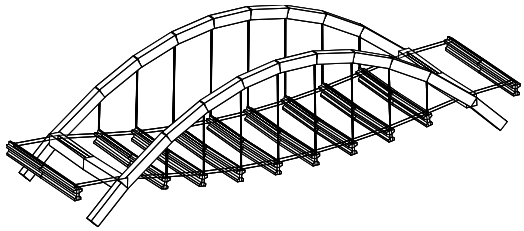

Fig. 18 Full FE fiber Model of Arch Bridge

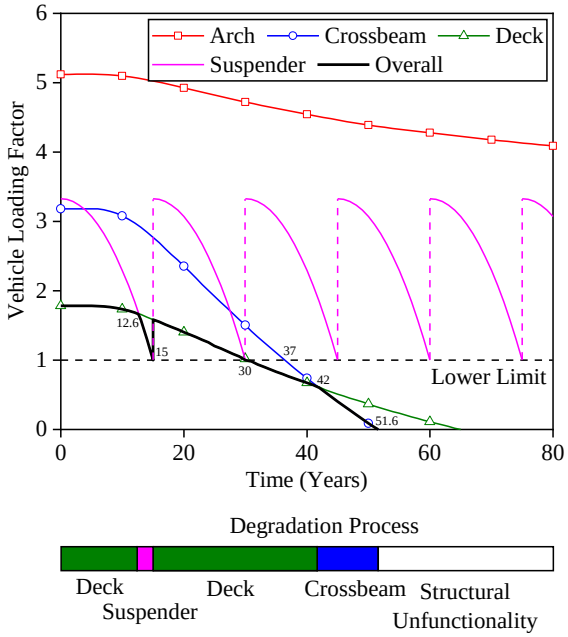

Fig. 19 Time evolution of structural capacity of members and overall structure and critical members

discontinuity of transferring the load effect from deck to arch (assuming the perfect working of abutment) and hereby dysfunction of whole structure. Therefore, the whole structural capacity is determined by the minimum capacity of each member under external load. The live load factors of four types of members over service life were obtained by numerical simulation, shown in colored solid lines in Fig. 19. Besides, a full FE model was created for verifying the time-variant minimum capacity of the bridge (Fig. 18). Obtained overall vehicle loading factor was drawn as black solid line in Fig. 19.

According to the result of numerical simulation, remaining structural capacity of arch was significantly higher than the other members. Besides, assuming complete corrosion of rebar and total spalling of concrete cover, the residual concrete section still provides remaining capacity as a beam-column. Thus arch could be ignored for further assessment regarding durability.

Considering normal operation for traffic loading, service stage of arch bridge was divided into normal stage ($\gamma \geq 1$) and dangerous stage ($\gamma < 1$) regarding vehicle loading factor. Detailed degradation process was listed in Table 3.

The above summary provided the basis for rehabilitation and maintenance of bridge. E.g., rehabilitation or entire replacement of crossbeam and deck at 30th year could be reasonable for structural safety.

Table 3 Deteriaration stages of overal structural capacity of arch bridge

Service Stage	Time (Years)	Weakest member	Degradation feature
Normal ($\gamma \geq 1$)	0~12.6	Deck	Being the weakest member, deck provided lower initial structural capacity. Its degradation caused by corrosion of rebar.
	12.6~15	Suspender	Suspender was considered to be replaced when attained its designed service life.
	15~30	Deck	Suspender was recovered after replacement.
Dangerous ($\gamma < 1$)	30~37	Deck	For any further degradation, deck was unsuitable for loading from traffic.
	37~42	Deck	Crossbeam became unsuitable for loading from traffic due to degradation. But deck remained the weakest member.
	42~51.6	Crossbeam	Due to faster degradation rate, crossbeam provided lower capacity than deck and became the weakest member until bridge was unsuitable for further service.

A summary was made according to the discussion in this section. The adopted FEM approach is simply based on beam theory, which was always applied in assessing of systematic structural performance and is unable to reveal the detailed deterioration of concrete structure. A better way for this problem is introducing refined FE model, such as three-dimensional model using 3D solid element. Another problem is stress effect on chloride diffusion within concrete. Tension or compression on concrete will accelerate or decelerate the diffusion of chloride, which was meaningful for discussion on stress distribution of concrete member under external load. Generally, it is significant for indeterminate structure since deterioration would cause further redistribution of internal force and structural capacity should be discussed in detail.

6. Conclusions

This paper presented a study on the corrosion model of steel rebar attacked by chloride ion within concrete and corresponding degradation of concrete structure based on the model discussed in this paper. A plane corrosion model was discussed theoretically and its key parameter was regressed by means of FE simulation. With a group of experimental data, a pitting model for localized corrosion was suggested. Moreover, durability of an aged reinforced concrete arch bridge was evaluated in macroscale. The conclusions of this study are summarized as follows:

(1) Global corrosion model is one focus discussed in this paper. Although the relationship between concentration of aggressive agent and corrosion was in microscopic

and rather complex, a simplified simulation based on the general law of corrosion from available natural corrosion experiments was applicable. The newly introduced Plane Corrosion Model improved the available Linear Corrosion Model for considering the dimension effect of rebar. Although assumptions for corrosion condition was still engaged, such as porosity of concrete, *w/c*, composition of cement, this damage model is useful for further research on corrosion of reinforcement and able to analysis the general law of performance degeneration of complex structures. Since it is still difficult to include all factors influence the diffusion process and corrosion process, the regression approach to obtain approximate principal coefficient adopted in this paper is suggested as an acceptable method.

(2) Pitting factor model provides the estimation on highly indeterminacy of local corrosion. Based on the collected literatures, a descending law of pitting factor with increase of average corrosion is clearly proved. However, pitting has been proved as highly uncertain along longitudinal direction of rebar. Deterministic law has rather a drawback of providing the most dangerous state of rebar.

(3) Practical reinforced concrete arch bridge was evaluated by means of the approach introduced in this paper, indicating the general descending law of structural performance regarding environmental attack and providing basis of rehabilitation strategy. Reasonable and accurate maintenance benefits from independent assessment for each types of members clearly revealing their own degradation laws.

(4) Compared with previous available approach for aged concrete structures, the approach proposed in this paper combined assessment on diffusion and structural analysis and provided the evaluation on time-dependent structural performance of reinforced concrete structures, which was considered to be theoretically practical and reliable for detailed analysis, though it was simplified due to several assumption and limited available experimental data.

Acknowledgements

This paper was sponsored by National Key Research and Development Program of China (2016YFC0701202), project supported by the National Natural Science Foundation of China (51508053) and project support by the Fundamental Research Funds for the Central Universities (106112014CDJZR200016), which were greatly appreciated by the authors.

Reference

Ascione, L., Berardi, V.P., Feo, L. and Mancusi, G. (2005), "A numerical evaluation of the interlaminar stress state in externally FRP plated RC beams", *Compos. Part B-Eng.*, **36**(1), 83-90.

Bastidas-Arteaga, E., Chateauneuf, A., Sánchez-Silva, M., Bressolette, P. and Schoefs, F. (2011), "A comprehensive probabilistic model of chloride ingress in unsaturated concrete", *Eng. Struct.*, **33**(3), 720-730.

Biondini, F., Bontempi, F., Frangopol, D.M. and Malerba, P.G. (2004), "Cellular automata approach to durability analysis of concrete structures in aggressive environments", *J. Struct. Eng.*, **130**(11), 1724-1737.

Biondini, F., Bontempi, F., Frangopol, D.M. and Malerba, P.G. (2006), "Probabilistic service life assessment and maintenance planning of concrete structures", *J. Struct. Eng*., ASCE, **132**(5), 810-825.

Biondini, F. and Vergani, M. (2012), "Damage modeling and nonlinear analysis of concrete bridges under corrosion", *Bridge Mainten. Saf. Manage. Resi. Sustain*., 949-957.

Cairns, J., Plizzari, G.A., Du, Y.G., Law, D.W. and Franzoni, C. (2005), "Mechanical properties of corrosion-damaged reinforcement", *ACI Mater. J.*, **102**(4), 256-264.

Castel, A., François, R. and Arliguie, G. (2000), "Mechanical behaviour of corroded reinforced concrete beams-Part 1: Experimental study of corroded beams", *Mater. Struct.*, **33**(233), 539-544.

Chen, A., Wang, Y., Wu, H. and Ruan, X. (2010), "Design service life determination for bridge structural elements", *J. Tongji Univ. (Nat. Sci.)*, **3**, 317-322.

Coronelli, D. and Gambarova, P. (2004), "Structural assessment of corroded reinforced concrete beams: Modeling guidelines", *J. Struct. Eng.*, ASCE, **130**(8), 1214-1224.

González, J.A. andrade, C., Alonso, C. and Feliu, S. (1995), "Comparison of rates of general corrosion and maximum pitting penetration on concrete embedded steel reinforcement", *Cement Concrete Res.*, **25**(2), 257-264.

Liu, T. and Weyers, R.W. (1998), "Modeling the dynamic corrosion process in chloride contaminated concrete structures", *Cement Concrete Res.*, **28**(3), 365-379.

Martín-Pérez, B., Zibara, H., Hooton, R.D. and Thomas, M.D.A. (2000), "A study of the effect of chloride binding on service life predictions", *Cement Concrete Res*., **30**(8), 1215-1223.

Papadakis, V.G. (2013), "Service life prediction of a reinforced concrete bridge exposed to chloride induced deterioration", *Adv. Concrete Constr.*, **1**(3), 201-213.

Roberge, P.R. (2008). *Corrosion Engineering Principles and Practice*, McGraw-Hill Education.

Rodriguez, J., Ortega, L.M. and Casal, J. (1997), "Load carrying capacity of concrete structures with corroded reinforcement", *Constr. Build. Mater.*, **11**(4), 239-248.

Sánchez, P.J., Huespe, A.E., Oliver, J. and Toro, S. (2010), "Mesoscopic model to simulate the mechanical behavior of reinforced concrete members affected by corrosion", *Int. J. Solid. Struct.*, **47**(5), 559-570.

Stewart, M.G. and Al-Harthy, A. (2008), "Pitting corrosion and structural reliability of corroding RC structures: Experimental data and probabilistic analysis", *Reliab. Eng. Syst. Saf.*, **93**(3), 373-382.

Thoft-Christensen, P. (2002), "Stochastic modelling of the diffusion coefficient for concrete", Department of Building Technology and Structural Engineering, Aalborg University, Aalborg.

Torres-Acosta Andrés, A. and Martı´nez-Madrid, M. (2003), "Residual life of corroding reinforced concrete structures in marine environment", *J. Mater. Civil Eng.*, **15**(4), 344-353.

Vidal, T., Castel, A. and François, R. (2004), "Analyzing crack width to predict corrosion in reinforced concrete", *Cement Concrete Res.*, **34**(1), 165-174.

Vidal, T., Castel, A. and François, R. (2007), "Corrosion process and structural performance of a 17 year old reinforced concrete beam stored in chloride environment", *Cement Concrete Res.*, **37**(11), 1551-1561.

Xu, J. and Chen, W. (2013), "Behavior of wires in parallel wire stayed cable under general corrosion effects", *J. Constr. Steel Res.*, **85**, 40-47.

Yu, L., François, R., Dang, V.H., L'Hostis, V. and Gagné, R. (2015), "Distribution of corrosion and pitting factor of steel in corroded RC beams", *Constr. Build. Mater.*, **95**, 384-392.

Yuan, Q., Shi, C., De Schutter, G., Audenaert, K. and Deng, D. (2009), "Chloride binding of cement-based materials subjected to external chloride environment-A review", *Constr. Build. Mater.*, **23**(1), 1-13.

Zhang, R., Castel, A. and François, R. (2009), "The corrosion pattern of reinforcement and its influence on serviceability of reinforced concrete members in chloride environment", *Cement Concrete Res.*, **39**(11), 1077-1086.

Zhang, R., Castel, A. and François, R. (2009), "Serviceability Limit State criteria based on steel-concrete bond loss for corroded reinforced concrete in chloride environment", *Mater. Struct.*, **42**(10), 1407.

Zhang, R., Castel, A. and François, R. (2010), "Concrete cover cracking with reinforcement corrosion of RC beam during chloride-induced corrosion process", *Cement Concrete Res.*, **40**(3), 415-425.

Zhang, Z. and Zhang, Q. (2017), "Self-healing ability of Engineered Cementitious Composites (ECC) under different exposure environments", *Constr. Build. Mater.*, **156**, 142-151.

Zhao, Y., Gao, X., Xu, C. and Jin, W. (2009), "Concrete surface chloride ion concentration varying with seasons in marine environment (Chinese)", *J. Zhejiang Univ. (Eng. Sci.)*, **43**(11), 2120-2124.

Zhu, W. and Francois, R. (2013), "Effect of corrosion pattern on the ductility of tensile reinforcement extracted from a 26-year-old corroded beam", *Adv. Concrete Constr.*, **1**(2), 121-136.

Zhu, W. and François, R. (2015), "Structural performance of RC beams in relation with the corroded period in chloride environment", *Mater. Struct.*, **48**(6), 1757-1769.

Zhu, W., François, R., Fang, Q. and Zhang, D. (2016), "Influence of long-term chloride diffusion in concrete and the resulting corrosion of reinforcement on the serviceability of RC beams", *Cement Concrete Compos.*, **71**, 144-152.

Zhu, W., François, R., Poon, C.S. and Dai, J.G. (2017), "Influences of corrosion degree and corrosion morphology on the ductility of steel reinforcement", *Constr. Build. Mater.*, **148**, 297-306.

CC